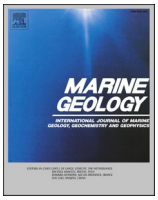
Marine Geology 473 (2024) 107322



Contents lists available at ScienceDirect

Marine Geology

journal homepage: www.elsevier.com/locate/margo



Research Article

Molecular and radiocarbon constraints on the fate of sedimentary organic carbon in a human-impacted river-dominated ocean margin

Chenglong Wang [a], Chuchu Zhang [a], Zhuoyue Zhang [a], Qihang Liao [a,b], Yang Zhang [a,c], Ning Wang [d,e], Yaping Wang [a], Xinqing Zou [a,b,*]

[a] School of Geographic and Oceanographic Sciences, Ministry of Education Key Laboratory for Coast and Island Development, Nanjing University, Nanjing, China
[b] Collaborative Innovation Center of South China Sea Studies, Nanjing University, Nanjing, China
[c] State Key Laboratory for Mineral Deposits Research, School of Earth Sciences and Engineering, Nanjing University, Nanjing, China
[d] State Key Laboratory of Isotope Geochemistry, CAS Center for Excellence in Deep Earth Science, Guangzhou Institute of Geochemistry, Chinese Academy of Sciences, Guangzhou 510640, China
[e] Southern Marine Science and Engineering Guangdong Laboratory (Guangzhou), Guangzhou 511458, China

ARTICLE INFO

Editor: Edward Anthony

Keywords:
River-dominated Ocean margins
Hydrodynamic sorting
Human perturbations
Mineral protection
Molecular biomarkers
Dual carbon isotope

ABSTRACT

Organic carbon (OC) burial in river-dominated ocean margins plays a pivotal role in the global carbon cycle, impacting atmospheric CO_2 levels over the long term. Despite its significance, uncertainties persist regarding the influence of external environmental factors and intrinsic properties on sedimentary OC. In this study, we conducted a comprehensive analysis of surface sediments from the East China Sea, examining geochemical properties (including total OC content [TOC], $\Delta^{14}C$, $\delta^{13}C$, and C/N ratio), terrestrial biomarkers (*n*-alkanes), and mineral properties (such as specific surface area, Al/Si ratio, and mineral composition). Our aim was to shed light on the fate of sedimentary OC.

The surface sediment's $\Delta^{14}C$ values displayed significant spatial heterogeneity, delineating four distinct subregions. Strong positive correlations (all $p < 0.01$) were found between the $\Delta^{14}C$ values and fine-grained sediments, specific surface area, and clay minerals, suggesting the potentially pivotal role of mineral protection in shaping the fate of sedimentary OC. The proportion of terrestrial OC gradually decreased towards the south, while marine OC proportion increased, corresponding to the enrichment of $\Delta^{14}C$. The co-variation of $\Delta^{14}C$ values, mineral properties, and OC source proportions suggests that terrestrial OC may undergo progressive replacement by marine OC during southward transport. Temporal variations in $\Delta^{14}C$ values indicated that seabed erosion led to a significant increase in $\Delta^{14}C$ values ($p < 0.01$) in the coastal mud belt, a phenomenon likely common in river-dominated ocean margins globally due to the new sediment cycle during the Anthropocene.

1. Introduction

Ocean margins play a crucial role in the global carbon cycle by receiving significant amounts of terrestrial and marine organic carbon (OC), particularly in river-dominated ocean margins (RiOMars) (Bauer et al., 2013; Regnier et al., 2013; Canuel and Hardison, 2016). Globally, rivers transport approximately 400 Tg C yr^{-1} of OC to the ocean, with approximately 200 Tg C yr^{-1} being particulate organic carbon (POC) (Ludwig et al., 1996). However, uncertainties persist regarding the fate of OC in RiOMars, influenced by OC sources and activity (Bianchi, 2011; Blair and Aller, 2012), mineral protection and selective preservation (Huguet et al., 2008; Hemingway et al., 2019), as well as physical, chemical, and biological processes (Carreira et al., 2011; Karlsson et al., 2015; Bao et al., 2019). Furthermore, different hydrodynamic conditions and transport pathways significantly influence the fate of sedimentary OC (Bröder et al., 2018; Ausín et al., 2021; Wang et al., 2022a). For example, hydrodynamic processes play a key role in regulating the aging of OC during lateral transport (Bao et al., 2018a, 2018b; Wei et al., 2020). Consequently, the fate of sedimentary OC in RiOMars, characterized by high dynamics and heterogeneity, is intricate due to spatial variability in sediment transport processes and OC inputs (Bao et al., 2016; van der Voort et al., 2018; Ausín et al., 2021).

* Corresponding author at: School of Geographic and Oceanographic Sciences, Ministry of Education Key Laboratory for Coast and Island Development, Nanjing University, Nanjing, China.
E-mail address: zouxq@nju.edu.cn (X. Zou).

https://doi.org/10.1016/j.margeo.2024.107322
Received 15 October 2023; Received in revised form 19 April 2024; Accepted 21 May 2024
Available online 22 May 2024
0025-3227/© 2024 Elsevier B.V. All rights are reserved, including those for text and data mining, AI training, and similar technologies.

Anthropogenic perturbations exert a significant influence on the transport of terrestrial organic carbon (OC_{terr}) from land to the ocean, leading to changes in OC sources, composition, and flux (Bauer et al., 2013; Regnier et al., 2013; Maavara et al., 2017). Notably, reservoirs intercept substantial amounts of POC, disrupting the transport of OC_{terr} and causing notable shifts in carbon stocks along coastal margins (Wang et al., 2020a). These altered sediment loads also impact the sedimentary environment, modifying sediment components within RiOMars (Maloney et al., 2018; Gao et al., 2019), thus profoundly influencing the fate of sedimentary OC (Wang et al., 2020a, 2022a). Consequently, anthropogenic perturbations introduce greater complexity to the fate of sedimentary OC in RiOMars, despite our incomplete understanding.

In recent years, there has been a growing interest in understanding the fate of sedimentary OC in the East China Sea (ECS). Substantial progress has been achieved using various geochemical methods, including the analysis of total OC content/total nitrogen content (C/N) ratio, $\delta^{13}C$, and biomarkers such as *n*-alkanes and lignin (Hu et al., 2012; Wu et al., 2013; Yao et al., 2015; Wang et al., 2022a). Moreover, natural radiocarbon (^{14}C) has emerged as a pivotal tool for investigating OC processing in the ECS, offering valuable insights into its origin and fate in marine sediments (Bao et al., 2016, 2018a, 2018b, 2019; Sun et al., 2021, 2022; Chu et al., 2022; Zhao et al., 2023). Factors such as organo-mineral interactions and hydrodynamic processes have been identified as key determinants of sedimentary OC fate (Bao et al., 2018a, 2018b; Wei et al., 2020; Chu et al., 2022). Specifically, Bao et al. (2018a, 2018b) proposed that hydrodynamic processes influence ^{14}C content through OC aging during lateral transport and selective degradation of OC associated with sediment (re)mobilization. However, these conclusions were drawn from the relationship between ^{14}C content and grain size, and direct evidence of mineralogical and OC degradation indexes is still lacking.

Furthermore, river damming has led to an 80% reduction in sediment loads within the Changjiang River basin (Guo et al., 2019), resulting in a 90% decline in allochthonous POC export and a 54% increase in autochthonous contribution (Wang et al., 2022b). This diminished sediment supply has triggered seabed erosion in the estuary, extending to the distal mud belt (Yang et al., 2018; Gao et al., 2019), potentially subjecting sedimentary OC to ongoing reworking, exposure to oxygen, and degradation via novel erosional processes (Blair and Aller, 2012; Bao et al., 2019; Wang et al., 2022a). Additionally, dam construction in the Changjiang River basin has also reduced the deposition flux of sedimentary OC in the estuarine–inner shelf areas of the ECS by 48% (Wang et al., 2020a). These alterations have complicated the fate of sedimentary OC in the estuarine–inner shelf areas of the ECS, prompting the need for further research.

Previous studies have identified spatial heterogeneity in the ^{14}C content of OC in the ECS, attributed to lateral transport and selective degradation (Bao et al., 2018a, 2018b, 2019). However, understanding the impacts of changes in OC provenance and degradation on sedimentary OC fate in the ECS remains incomplete. This knowledge gap impedes our understanding of the underlying causes of spatial ^{14}C content heterogeneity in ECS sediments. The present study extends previous research, examining ^{14}C content, specific surface area (SSA), grain size, elemental and mineral composition, bulk OC properties (including total organic carbon (TOC), C/N ratio, and $\delta^{13}C$), and biomarkers (*n*-alkanes) in surface sediments of the estuarine-inner shelf ECS areas. Utilizing mineralogy and OC degradation indexes, we aim to elucidate sedimentary OC dispersal and aging in this region. Additionally, we compare ^{14}C contents of surface sediments collected from the ECS in 2007 and 2011 to investigate temporal variations in sedimentary OC fate.

2. Materials and methods

2.1. Study area and sampling sites

The ECS exhibits typical characteristics of a RiOMars, boasting a vast continental shelf that receives substantial sediment influx from the Changjiang River, the longest river in Eurasia. Its primary circulation features include the Changjiang diluted water (CDW), the Zhejiang–Fujian coastal current (ZFCC), and the Taiwan warm current (TWC) (Fig. 1a). The significant sediment load from the Changjiang River is predominantly transported southwards, leading to the formation of two nearshore mud deposits: the Changjiang subaqueous delta mud deposit and the Zhejiang–Fujian coastal mud belt (ZFCMB) (Fig. 1b, Liu et al., 2007). In the outer Changjiang River Estuary (CRE, Fig. 1b), a tidal sand ridge known as the "Yangtze Shoal" exists, mainly comprised of relict sand formed during post-glacial transgression (Chen et al., 1986; Liu et al., 2020). Since the 1980s, the construction of over 50,000 reservoirs in the Changjiang River basin (Yang et al., 2011) has led to the interception of sediment at a rate of 453 Mt. yr^{-1} (Gao et al., 2018). These substantial reductions in sediment loads have induced severe seabed erosion, particularly in the CRE and even extending to the Yangtze Shoal (Yang et al., 2018; Gao et al., 2019). For this study, a total of 23 surface sediment samples (0–2 cm) were collected from the estuarine–inner shelf areas of the ECS using a box corer (Fig. 1b) between March and May 2018. All samples were promptly frozen (−20 °C) for subsequent analysis.

2.2. Sample analysis

2.2.1. Radiocarbon measurement

Freeze-dried surface sediments were pretreated with 1.0 N HCl at 60 °C for 1 h, then samples were rinsed and freeze-dried. Aliquots containing approximately 1 mg OC were combusted into gaseous CO_2 in sealed vacuumed quartz tubes with silver and CuO at 850 °C, purified and graphitized using method proposed by Xu et al. (2007). The sampled preparation was carried out by the state key Laboratory of Isotopic Geochemistry, and the graphite targets were measured using a compact 0.5 MeV NEC accelerator mass spectrometer at State Key Laboratory of Organic Geochemistry, Guangzhou Institute of Geochemistry, Chinese Academy of Sciences (Zhu et al., 2015). Total uncertainties of the radiocarbon treatments and measurements ($\Delta^{14}C$) were < 3.0 ‰, based on 6 primary standards with the same treatment in each wheel. Radiocarbon results of sediments were reported as F_m and $\Delta^{14}C$ values (‰) (Stuiver and Polach, 1977).

2.2.2. XRF analysis

Approximately 0.8 g of freeze-dried and homogenized sediment powder was mixed with 7 g of fusion (lithium tetraborate 67% + lithium metaborate 33%) inside a platinum-gold crucible, then heated to 1050 °C for 5 min until the sample melted and became homogenized. The melt was cast into a mold and cooled for measurement on a wavelength-dispersive sequential ARL PERFORM'X XRF spectrometer (Thermo Fisher, USA) at the Analyzing and Testing Center of the Third Institute of Oceanography, Ministry of Natural Resources. To monitor the analytical precision and accuracy, three sets of sample duplicates were assessed. The relative error was <0.6% for major elements, demonstrating the reliability of the XRF analysis. In this study, only SiO_2 and Al_2O_3 data are reported.

2.2.3. X-ray crystallography (XRD) analysis

Mineral composition was determined by XRD analysis. Briefly, 1 g of the <63 μm sediment fraction was wet-milled in ethanol to <20 μm using a McCrone Micronising mill. The resulting <20 μm fraction was dried overnight (60 °C) and further powdered and homogenized using a mini mill. Randomly oriented powdered specimens were subsequently prepared. The powdered material was introduced into a sample holder

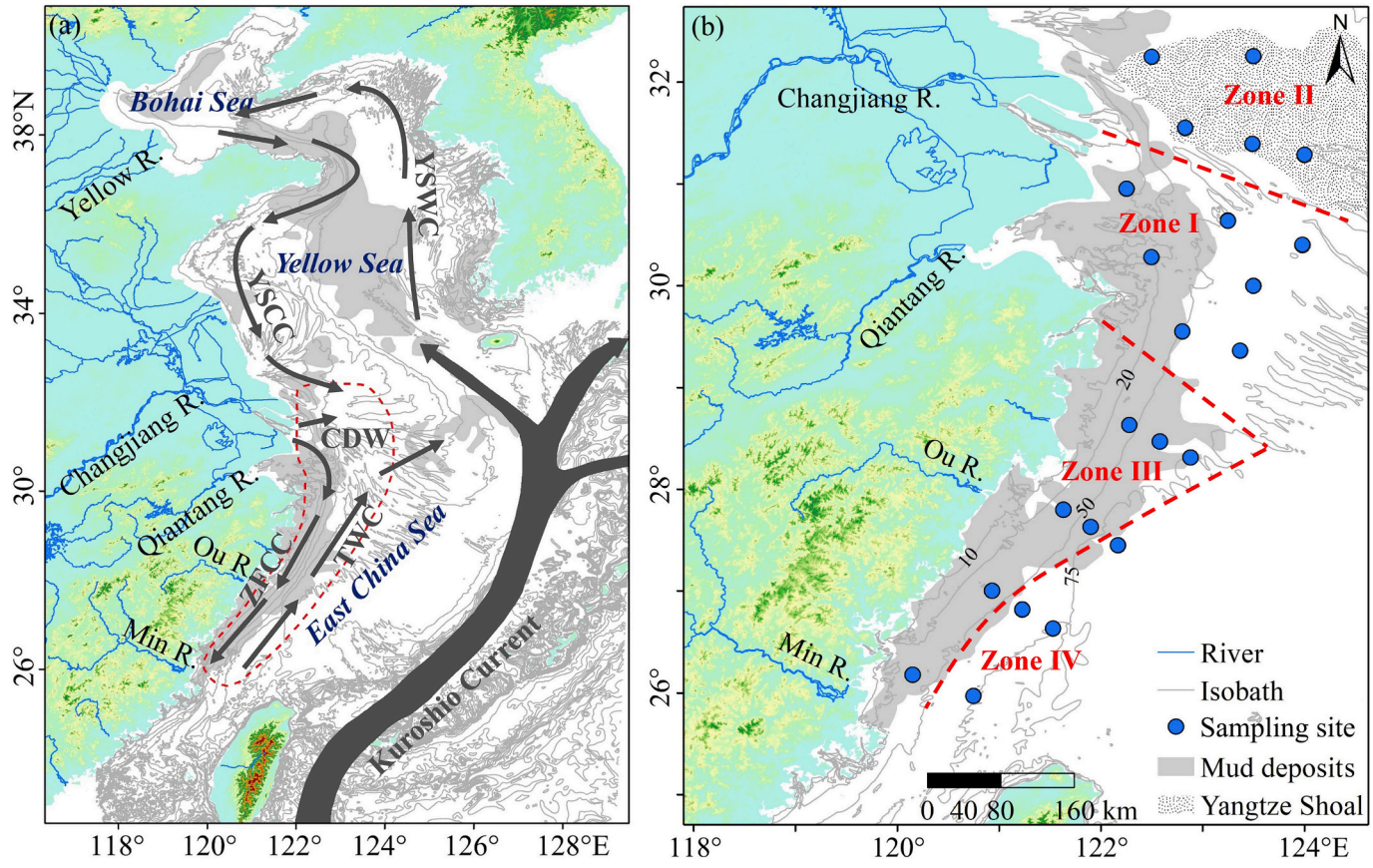


Fig. 1. Study area within the East China Sea showing (a) major oceanic currents including the Changjiang-diluted water (CDW), Zhejiang-Fujian coastal current (ZFCC), Taiwan warm current (TWC), Yellow Sea coastal current (YSCC), Yellow Sea warm current (YSWC), and Kuroshio current; (b) Locations of sampling sites in the estuarine-inner shelf areas of the ECS. Light gray patch represents the mud deposits; Zone I: inner CRE, Zone II: Yangtze Shoal, Zone III: ZFCMB, Zone IV: Taiwan impact Zone. (For interpretation of the references to colour in this figure legend, the reader is referred to the web version of this article.)

for packing, and a flat surface was formed using a razor blade to minimize preferential orientation. XRD measurements were performed on a Bruker AXS D8 Theta-Theta diffractometer with a SolX detector using Co Kα radiation. The irradiated sample length was held constant at 18 mm using an automatic θ-compensating divergence slit. Powdered specimens were measured from 2° to 80° 2θ with a step size of 0.02° and 4 s/step counting time. The qualitative phase composition was determined with the DIFFRACplus software (BRUKER AXS). Quantification of minerals was achieved with BGMN/AutoQuan software using Rietveld refinement. The minerals detected in this study included quartz, dolomite, albite, orthoclase, tremolite, calcite, and phyllosilicates (chlorite, kaolinite, illite, and smectite).

2.3. Dual carbon isotope model

A dual carbon isotope model based on the $\delta^{13}C$ and $\Delta^{14}C$ values was used to constrain the proportions of three OC pools, i.e., petrogenic OC (OC_{petro}, f_{petro}), pre-aged soil OC ($OC_{pre\text{-}aged}$, $f_{pre\text{-}aged}$), and marine primary production (OC_{mar}, f_{mar}) of surface sediment collected in 2018 (n = 23). OC_{petro} originating from bedrock weathering exerts no effect on atmospheric CO_2 during recycling and reburial (Galy et al., 2008). $OC_{pre\text{-}aged}$ has been buried in soil for thousands of years (Drenzek et al., 2007), and OC_{mar} is modern carbon produced by photosynthesis. The relative fractional contribution of three OC pools to sedimentary OC was estimated using Eqs. (1)–(3):

$$\delta^{13}C_{TOC} = f_{petro} \times \delta^{13}C_{petro} + f_{pre-aged} \times \delta^{13}C_{pre-aged} + f_{mar} \times \delta^{13}C_{mar} \quad (1)$$

$$\Delta^{14}C_{TOC} = f_{petro} \times \Delta^{14}C_{petro} + f_{pre-aged} \times \Delta^{14}C_{pre-aged} + f_{mar} \times \Delta^{14}C_{mar} \quad (2)$$

$$1 = f_{petro} + f_{pre-aged} + f_{mar} \quad (3)$$

where $\delta^{13}C_{TOC}$ and $\Delta^{14}C_{TOC}$ are the measured values of sediment samples. The $\delta^{13}C$ and $\Delta^{14}C$ values of endmembers (OC_{petro}, $OC_{pre\text{-}aged}$, and OC_{mar}) were constrained by carbon isotopic compositions provided by previous studies and listed in Table S1. To account for the variability of the endmember values, a Monte Carlo (MC) approach was used, using in-house Matlab (ver. 2014b) scripts. A total of 1,000,000 iterations were run for each sample, with a burn-in (initial search time) of 10,000 and a data thinning (removal of correlations between iterations) of 10. The variability between several MC runs is much smaller than the standard deviations of the estimated parameter distributions. Running the same simulation 10 times provides a relative standard deviation of <1% for the estimated parameter value. We therefore conclude that the convergence of the simulations does not affect our interpretations. The MC simulations are very robust with respect to the choice of input parameters: regardless of their choice the runs converge within the burn-in phase. The stochastic perturbations are tuned to meet the well-established criterion of an acceptance rate of ~0.23, which theoretically has been found to be an optimal condition for a broad range of MC algorithms.

2.4. Data collection

The datasets of sedimentary parameters (surficial sediment grain size, and components [clay, silt, and sand contents]) and bulk OC properties (TOC content, C/N ratio, and $\delta^{13}C$) were obtained by Wang et al. (2020a). The datasets of n-alkanes concentration and SSA were collected from Wang et al. (2022a). High molecular weight (HMW) n-

alkanes originate from terrestrial higher plant waxes (Eglinton and Hamilton, 1967), and their carbon preference index (CPI, CPI_{25-33}) serve as markers of OC maturity and reflect its relative degradation state (Fahl and Stein, 1997; Vonk et al., 2012). $\Delta^{14}C$ values of surficial sediments collected in 2007, 2011 and 2017 were obtained by Bao et al. (2016) and Fu et al. (2022).

2.5. Statistics

Statistical analyses were conducted using SPSS software (version 22.0; SPSS Institute, USA). Pearson correlation analysis, implemented in SPSS, was employed to assess the relationships between parameters. The Shapiro-Wilk test was utilized to assess the normality of the ^{14}C content data for the three time periods (2007, 2011, 2018). If the data followed a normal distribution, significance differences were evaluated using one-way ANOVA analysis; otherwise, non-parametric Kruskal-Wallis analysis was employed (all analyses conducted at a confidence level of 0.05).

3. Results

3.1. Radiocarbon activities

The surface sediment $\Delta^{14}C$ values ranged from −254.6‰ to −570.8‰ (mean: −348.6 ± 80.2‰; $n = 23$, Table S2), corresponding to conventional ^{14}C ages ranging from 2290 to 6725 years before present (yr BP), with an average of 3504 ± 1215 yr BP (Table S2). The Yangtze Shoal and the outer south ZFCMB exhibited relatively low $\Delta^{14}C$ values, as illustrated in Fig. 2a. In contrast, slightly higher $\Delta^{14}C$ values were observed in the inner CRE and ZFCMB (Fig. 2a).

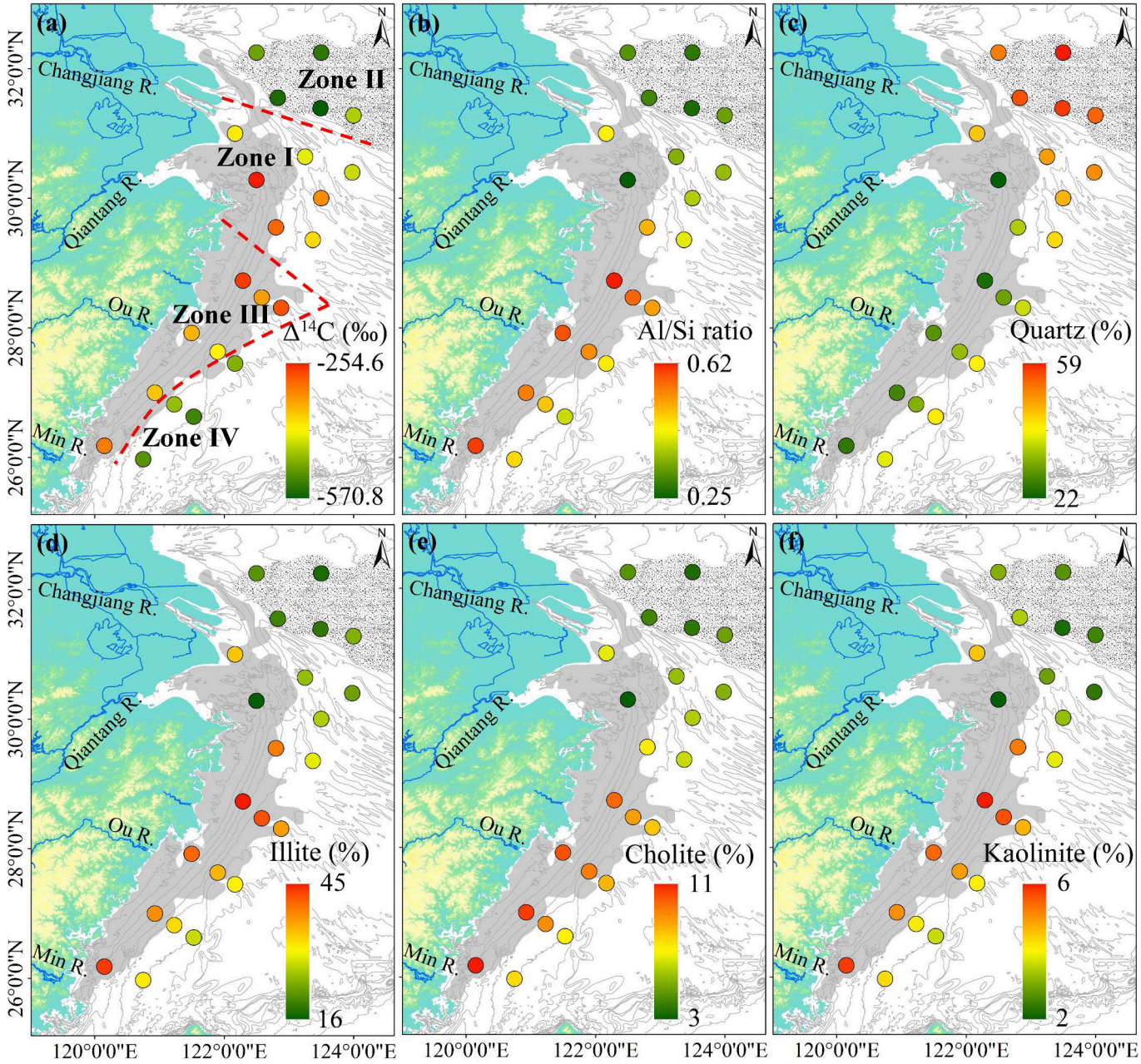


Fig. 2. Spatial distribution of radiocarbon contents and mineral characteristics of surficial sediments; (a) $\Delta^{14}C$ value, (b) Al/Si ratio; (c) quartz content, (d) illite content, (e) chlorite content, (f) kaolinite content, patches with light gray represent mud deposits. Zone I: inner CRE, Zone II: Yangtze Shoal, Zone III: ZFCMB, Zone IV: Taiwan impact Zone.

3.2. Mineralogical characteristics

The Al_2O_3 to SiO_2 (Al/Si) ratio in surface sediments ranged from 0.14 to 0.30 (mean: 0.21 ± 0.05; Fig. 2b), exhibiting a similar variation to that observed for grain size. Quartz was the predominant mineral detected in the sediments, ranging from 25.33% to 55.56% (mean: 38.45 ± 9.41%; Fig. 2c), followed by clay minerals, which ranged from 24.47% to 63.12% (mean: 45.09 ± 11.23%). Among the clay minerals, illite was the most abundant, with an average of 32.35 ± 7.06% (Fig. 2d), followed by chlorite (mean: 7.50 ± 2.13%; Fig. 2e) and kaolinite (mean: 5.23 ± 2.04%; Fig. 2f).

3.3. Model-derived OC sources

A dual carbon isotope model was employed to identify three distinct sources of OC and their corresponding contributions. Table S3 presents the model-derived estimates detailing the relative proportions of OC_{petro}, $OC_{pre\text{-}aged}$, and OC_{mar} across the ECS and its sub-regions. Among these sources, OC_{petro} constituted the smallest fraction of sedimentary OC in the ECS, varying from 12% to 50% (mean: 25 ± 11%; Fig. 3a and Table S3). Following closely was OC_{mar}, contributing between 13% and 52% (mean: 33 ± 11%; Fig. 3c and Table S3), with $OC_{pre\text{-}aged}$ spanning from 16% to 69% (mean: 42 ± 14%; Fig. 3b and Table S3).

4. Discussion

4.1. Spatial heterogeneity of $\Delta^{14}C$ values in the ECS

The surface sediments within the estuarine-inner shelf regions of the ECS showcased pronounced spatial heterogeneity in $\Delta^{14}C$ values, indicative of distinct depositional environments and carbon dynamics. In a preceding study, van der Voort et al. (2018) employed a novel numerical clustering algorithm to categorize OC dynamics within the ECS into three zones: the East China Sea-Yellow Sea shelf, the Changjiang impact zone, and the Taiwan impact zone. Nevertheless, in our investigation, we further partitioned the Changjiang impact zone into two sub-regions, specifically the CRE region and ZFCMB, owing to discernible alterations in depositional conditions stemming from a marked reduction in riverine input (Fig. 1b). Through an examination of the spatial variations in $\Delta^{14}C$ values and OC characteristics across these four delineated regions, we ascertained that OC provenance and hydrodynamic sorting emerged as the principal factors governing the fate of sedimentary OC within the ECS.

Zone I (the CRE region, $n = 7$) is delineated by the Changjiang outflow and the directional influence of the sedimentary plume affected by CDW. Sediments within this region exhibit relatively high $\Delta^{14}C$ values (−311.11 ± 35.47‰), TOC content (0.35 ± 0.14%), and C/N ratio (7.24 ± 0.36%), along with lower $\delta^{13}C$ values (−22.24 ± 0.80‰) (Table S4, Fig. 2, Wang et al., 2020a). This area experiences significant impacts from Changjiang River discharge, displaying a distinct terrestrial signature in the composition of OC (evidenced by a high C/N ratio and low $\delta^{13}C$ values). $\Delta^{14}C$ values in the CRE region exhibit an increasing trend from the estuary towards offshore locations (Fig. 2a). Previous studies have indicated that POC discharged from the Changjiang River typically exhibits relatively high $\Delta^{14}C$ values (−114.25 ± 9.42‰, Wang et al., 2012). Recent research has further revealed that a substantial portion of Changjiang-derived POC consists of "labile" fractions prone to degradation or loss due to frequent physical reworking coupled with rapid Fe redox cycling along the estuarine continuum (Sun et al., 2022; Zhao et al., 2023). As distance from the estuary increases, there is continuous supplementation of "labile" marine OC (OC_{mar}), characterized by a lower C/N ratio and higher $\delta^{13}C$ values. This phenomenon may contribute to the observed increase in $\Delta^{14}C$ values from the estuary to offshore areas. Additionally, Zone I experiences a high frequency of algal blooms and hypoxia (Zhu et al., 2011; Wang et al., 2016). Thus, the elevated primary productivity, which supplies fresh OC_{mar}, may serve as another factor influencing the enrichment of $\Delta^{14}C$ values.

Zone II (Yangtze Shoal region, $n = 5$) displays the lowest $\Delta^{14}C$ values (−476.54 ± 79.58‰), TOC content (0.10 ± 0.09%), and C/N ratio (4.59 ± 2.27), along with the highest $\delta^{13}C$ values (−21.55 ± 0.68‰) (Table S4, Fig. 2). Previous studies have indicated that the composition of Yangtze Shoal is primarily influenced by strong tidal currents and mainly comprises relict sand without modern deposits (Li et al., 2014a, 2014b; Liu et al., 2020). This shoal formed during the post-glacial transgression, resulting in a higher concentration of ^{14}C-depleted

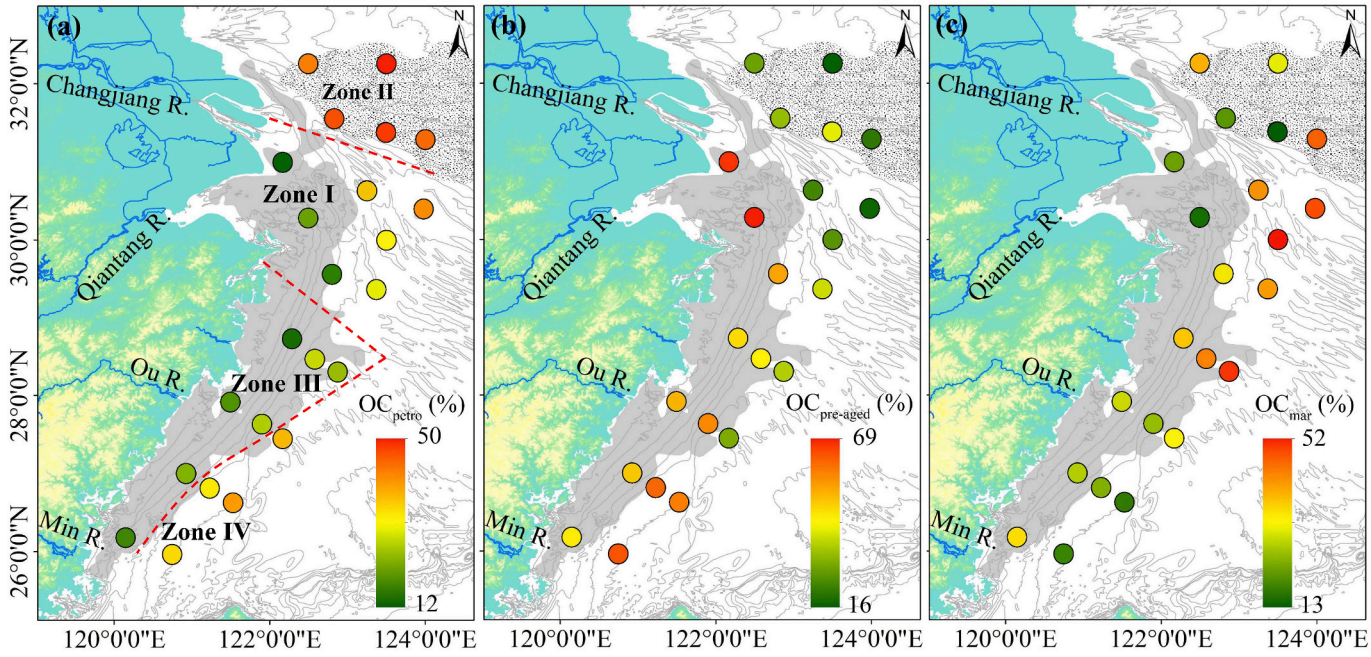


Fig. 3. Spatial variations in relative contributions of sedimentary OC in the ECS; (a) OC_{petro}, (b) $OC_{pre\text{-}aged}$, and (c) OC_{mar}. patches with light gray represent mud deposits. Zone I: CRE, Zone II: Yangtze Shoal, Zone III: ZFCMB, Zone IV: Taiwan impact Zone.

carbon in the Yangtze Shoal region.

Zone III (ZFCMB region, n = 7) encompasses an extensive mobile mud belt that parallels the Zhejiang-Fujian coastline. It is distinguished by the highest $\Delta^{14}C$ values (−276.81 ± 18.56‰) and TOC content (0.61 ± 0.13%), as well as relatively elevated C/N ratios (7.24 ± 0.33) and low $\delta^{13}C$ values (−22.42 ± 0.25‰) (Table S4, Fig. 2). Compared to the CRE region, the $\Delta^{14}C$ values in the ZFCMB region are notably higher (Shapiro-Wilk test, all $p > 0.05$; one-way ANOVA analysis: $F = 21.19$, $p < 0.05$). The $\Delta^{14}C$ values in the ZFCMB are also influenced by the discharge of the Changjiang River and are closer to the younger Changjiang-derived sediments ($\Delta^{14}C = -114.3 \pm 9.4$‰, Wang et al., 2012). Particularly, the northern sector of the ZFCMB exhibits the highest $\Delta^{14}C$ values (Fig. 2), coinciding with the cross-shelf penetrating front identified by Yuan and Hsueh (2010). Furthermore, the region with enriched $\Delta^{14}C$ values in the ZFCMB (between 28° and 30° N) aligns with an upwelling area characterized by high primary productivity (Chen et al., 2004; Hu and Wang, 2016).

Zone IV (Taiwan impact zone, $n = 4$) lies to the east of the southern ZFCMB and intersects with the path of the TWC (Fig. 1a). It is characterized by relatively lower $\Delta^{14}C$ values (−400.15 ± 22.88‰), TOC contents (0.37 ± 0.09%), C/N ratios (6.43 ± 0.68), and the lowest $\delta^{13}C$ values (−22.55 ± 0.39‰) (Table S4, Fig. 2). The $\Delta^{14}C$ values of surface sediments in the Taiwan impact zone are more depleted compared to those in the adjacent ZFCMB zone, likely due to the influx of ^{14}C-depleted and ^{13}C-depleted organic carbon from Taiwan Island, transported northward by the TWC (as noted by Kao et al., 2014; Bao et al., 2016). Additionally, the presence of the TWC serves as a barrier, impeding the transport of young Changjiang-derived sediments into Zone IV.

4.2. Provenance of sedimentary OC in the ECS

Spatially, the relative contribution of OC_{petro} to sedimentary OC exhibits an increasing trend moving away from the coast, with the highest values found in the outer CRE (Zone II), coinciding with the location of the "Yangtze Shoal" (Fig. 3a). The sediments within the "Yangtze Shoal" consist of relict sands formed during a post-glacial transgression and have been exposed to oxygen for an extended period, resulting in low TOC content and depleted ^{14}C values. Additionally, a high proportion of OC_{petro} is observed in the outer zone of the ZFCMB (Zone IV) (Fig. 3a), where the influence of older OC derived from Taiwan is significant. In contrast, nearshore areas, especially within the CRE region, exhibit a high proportion of $OC_{pre\text{-}aged}$ (Fig. 3b). The spatial distribution of $OC_{pre\text{-}aged}$ within the CRE region decreases from the estuary to offshore, corresponding to a diminishing influence of riverine input (Fig. 3b). Similarly, vertically along the coast, the contribution of $OC_{pre\text{-}aged}$ gradually diminishes from the coast to offshore (Fig. 3b). Conversely, the contribution of OC_{mar} shows an increasing trend from the coast to offshore (Fig. 3c), with the lowest proportion observed in the CRE region and the highest in the outer CRE (Fig. 3c). We propose that the diminishing influence of terrestrial input, coupled with the increasing impact of marine primary production, is likely the primary factor controlling the variations in OC_{mar}. Furthermore, there is a relatively low proportion of OC_{mar} in the outer ZFCMB (Fig. 3c), possibly due to dilution from inputs originating from Taiwan.

4.3. Mechanistic control of the diverse sedimentary OC fates in the ECS

4.3.1. Hydrodynamic controls on the spatial heterogeneity of $\Delta^{14}C$ values

The spatial heterogeneity of $\Delta^{14}C$ values in coastal margins is often attributed to hydrodynamic processes, which can be assessed by examining the relationships between $\Delta^{14}C$ values and particle size. In this study, Pearson correlation analysis was conducted between $\Delta^{14}C$ values and sediment grain size/components to investigate the impact of hydrodynamic sorting on the fate of sedimentary OC. The results revealed a significant positive correlation between $\Delta^{14}C$ values and sediment grain size ($R^2 = 0.55$, $p < 0.01$), as well as fine-grained sediments ($R^2 = 0.65$, $p < 0.01$ for silt content) (Fig. 4a, b). Conversely, a significant negative correlation was found between $\Delta^{14}C$ values and sand content ($R^2 = 0.65$, $p < 0.01$) (Fig. 4c). Notably, these correlations were absent in samples collected in 2007, consistent with previous findings on other indices such as organic pollutants and terrestrial biomarkers in the study area (Wang et al., 2020b, 2020c, 2022a). The absence of coarse sediments in 2007 likely explains these observations (Lin et al., 2013; Wang et al., 2020b, 2020c). However, there are limitations, as the sediments here are continuous and not specifically studied for specific grain sizes. More comprehensive information could be obtained from extensive surveys of different grain size fractions, particularly considering the influence of hydrodynamic processes (Bao et al., 2019).

The Pearson correlation analysis revealed an enrichment of $\Delta^{14}C$ values in fine-grained sediments, while depletion was observed in coarse-grained sediments (Fig. 4a–c). Bao et al. (2019) proposed that the $\Delta^{14}C$ values in coastal mud deposits are influenced by resuspension processes. Accordingly, both fine-grained and coarse-grained sediments exhibit relatively enriched $\Delta^{14}C$ values, whereas the "sortable silt" fraction (20–63 μm) shows a relatively depleted $\Delta^{14}C$ value. Due to the influence of coastal currents, the "sortable silt" fraction, along with its associated OC, undergoes multiple cycles of resuspension and deposition during along-shelf transport (Bao et al., 2018a, 2018b, 2019). This prolonged transportation and exposure to oxygen contribute to the degradation and aging of sedimentary OC (Blair and Aller, 2012; Bröder et al., 2018), leading to the observed depletion of ^{14}C in the "sortable silt" fraction. However, it is noteworthy that this phenomenon was not observed in 2018, despite the occurrence of more significant seabed erosion and sediment re-suspension processes during this period compared to 2007 (Gao et al., 2019; Wang et al., 2020a).

Coastal currents play a significant role in sediment and associated OC transport along the shelf (Liu et al., 2007; Bao et al., 2018a, 2018b). Within our study area, sediments undergo multiple cycles of resuspension and deposition, leading to prolonged transport and exposure to oxygen for both sediments and associated OC (Blair and Aller, 2012; Bröder et al., 2018). To delve deeper into this phenomenon, we explored the correlations between the relative contents of different OC sources and the distance from the river mouth in the mud belt, primarily influenced by Changjiang-derived sediments (Fig. S1). As sediments journey from the river mouth to the Taiwan Strait, there's a decline in OC_{terr} (OC_{petro} and $OC_{pre\text{-}aged}$) content, indicative of continuous depletion due to cyclic resuspension/deposition (Bao et al., 2016) (Fig. S1a). Conversely, OC_{mar} content exhibits a southward increasing trend (Fig. S1b), implying a steady supplement of marine-derived OC. In the CRE region, two samples within the mud deposit display relatively high OC_{terr} content due to the significant influence of the Changjiang River. A previous study has demonstrated that OC derived from catchment soil and adsorbed on fine-grained particles was transported offshore, consistent with the variation trend of $OC_{pre\text{-}aged}$ (Fig. 3b).

Under the dynamic changes in the relative contributions of OC_{mar} and OC_{terr}, the $\Delta^{14}C$ values of sedimentary OC do not exhibit a monotonically decreasing trend due to degradation during transport (Fig. 4e). Instead, they demonstrate a decreasing trend as the distance from the river mouth increases, indicating a potentially greater influence of Taiwan-derived sediments in the southern ZFCMB. Even within the mud belt, the $\Delta^{14}C$ values appear to gradually increase away from the river mouth, though the correlation is not significant (Fig. S2). Furthermore, the TOC content in surface sediments also increases with southward transport distance (Fig. 4f). These findings suggest that the degradation of OC_{terr} due to cyclic resuspension/deposition may not be the primary factor driving the spatial variability of $\Delta^{14}C$ values in this region. Instead, the replenishment of young OC_{mar} may offset the depletion of $\Delta^{14}C$ caused by the degradation of OC_{terr} during southward transport. This compensatory effect even results in $\Delta^{14}C$ becoming more enriched with increasing transport distance, although this trend is not statistically significant. Additionally, the replenishment of OC_{mar} may also be an

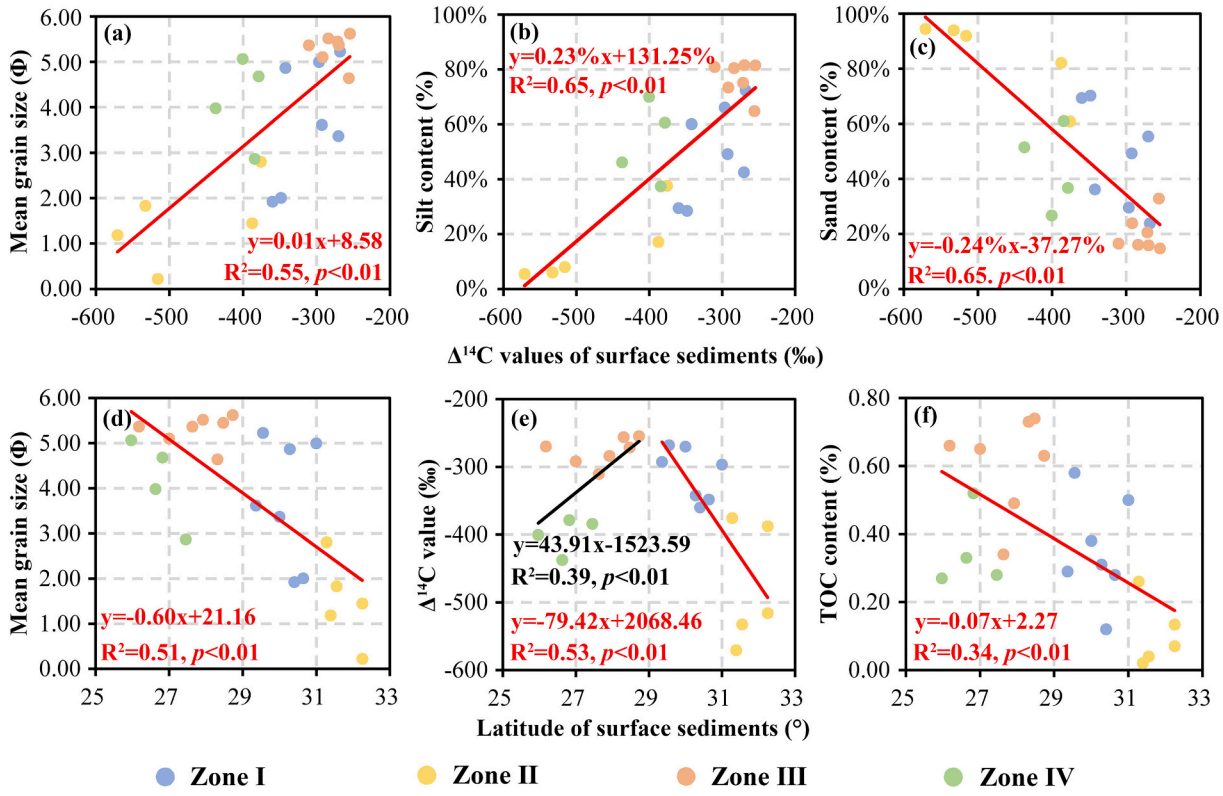


Fig. 4. Plots of $\Delta^{14}C$ value versus sediment grain size (a), silt content (b), and sand content (c); plots of latitude versus sediment grain size (d), ^{14}C age (e) and TOC content.

important factor contributing to the increasing trend of TOC content with transport distance.

4.3.2. *Mineralogical controls on the fate of sedimentary OC*

Mineral protection plays a crucial role in stabilizing and preserving sedimentary OC over the long term, often characterized by first-order relationships between SSA and OC content (Blattmann et al., 2019; Hemingway et al., 2019). Furthermore, the Al/Si ratio serves as an indicator of mineral protection, with a high ratio indicating the presence of Al-rich fine-grained minerals and a low ratio suggesting silicon-rich particles of coarse-grained minerals (Galy et al., 2008; Bouchez et al., 2011). Our results unveil a strong positive correlation between SSA and TOC content (Fig. 5a), indicating that minerals positively influence the preservation of sedimentary OC. Likewise, a significant positive correlation between TOC content and the Al/Si ratio confirms the covariation of TOC content with Al-rich fine-grained minerals (R^2 = 0.70, $p < 0.01$; Fig. 5c). To delve deeper into the mineralogical control on sedimentary OC preservation, we identified typical minerals. Interestingly, a robust negative correlation between TOC content and quartz content was observed (R^2 = 0.71, $p < 0.01$; Fig. 5e), suggesting that coarse-grained minerals have a lower capacity for adsorbing sedimentary OC. In contrast, TOC content exhibited strong positive correlations with clay minerals (Fig. 5g), such as illite ($R^2 = 0.68$, $p < 0.01$), chlorite ($R^2 = 0.68$, $p < 0.01$), and kaolinite ($R^2 = 0.51$, $p < 0.01$). These findings collectively underscore significant correlations between TOC content and mineral properties, suggesting that Al-rich fine-grained minerals possess a higher OC holding capacity.

We also investigated the relationships between $\Delta^{14}C$ values and mineral properties to discern the mechanism by which mineral protection influences OC aging. Our findings revealed a strong positive correlation between SSA and $\Delta^{14}C$ values (Fig. 5b), suggesting that minerals play a key role in preserving young OC. Similarly, a significant positive correlation between $\Delta^{14}C$ values and the Al/Si ratio confirmed the association of $\Delta^{14}C$ values with sediment grain size and mineralogy (R^2 = 0.66, $p < 0.01$; Fig. 5d). To further elucidate the mineralogical controls on OC aging in the ECS, we examined the relationships between $\Delta^{14}C$ values and typical minerals, including quartz and clay minerals. Pearson correlation analysis revealed a robust negative correlation between $\Delta^{14}C$ values and quartz content (R^2 = 0.82, $p < 0.01$, Fig. 5f), aligning with the Al/Si ratio and SSA findings. Conversely, strong positive correlations were observed between $\Delta^{14}C$ values and clay minerals (R^2 = 0.82, $p < 0.01$, Fig. 5h). These associations between $\Delta^{14}C$ values and mineral properties suggest that Al-rich fine-grained minerals are more inclined to adsorb relatively young sedimentary OC. Furthermore, if we can directly extract clay minerals for radiocarbon isotope analysis, we may obtain more direct evidence, offering deeper insights into the role of mineral protection in shaping the fate of sedimentary OC in marine environments.

To explore the adsorption preferences of minerals for sedimentary OC, we assessed the relationships between mineral properties and different OC sources in mud deposits (Fig. S3). Our findings revealed negative correlations between mineral properties and the proportion of OC_{terr}, possibly attributable to the degradation of OC_{terr} during transport (Fig. S3). In contrast, robust positive correlations were observed between mineral properties and the proportion of OC_{mar} (Fig. S3). Specifically, despite an increase in Al-rich fine-grained minerals, there was an increasing proportion of OC_{mar} and a decreasing proportion of OC_{terr}. This phenomenon, akin to observations in the northeastern South China Sea, where the loss and replacement of OC_{terr} initially associated with aluminosilicate mineral surfaces were noted, finds support in our results (Blattmann et al., 2019). Our findings lend credence to this hypothesis by demonstrating that the amount of OC_{terr} adsorbed on mineral surfaces gradually decreases with an increase in transport distance, thereby providing more adsorption sites for OC_{mar}. Hence, our study suggests that mineral protection may play a critical role in controlling the preservation and aging of sedimentary OC in marine sediments.

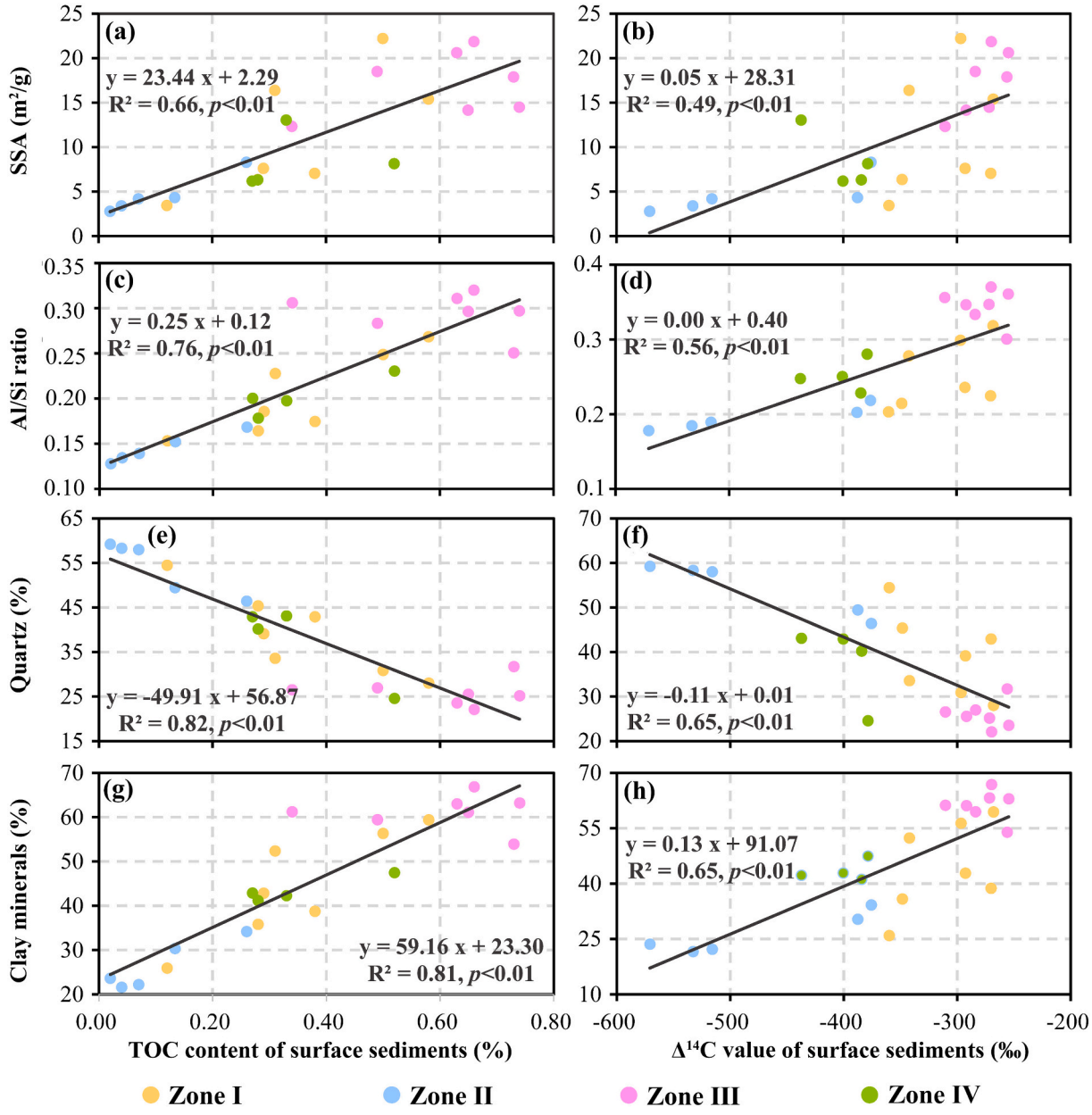


Fig. 5. Plots of TOC content (left) and $\Delta^{14}C$ values (right) versus mineral properties of sediments from the ECS; (a, b) SSA, (c, d) Al/Si ratios, (e, f) Quartz content, (g, h) content of clay minerals (illite + chlorite + kaolinate).

4.3.3. Assessing the effects of intrinsic properties on the fate of sedimentary OC

In addition to external hydrodynamic processes and mineral protection, intrinsic factors determining the degradation of sedimentary OC are expected to primarily influence the distribution of $\Delta^{14}C$ in surface sediments from RiOMars (Wei et al., 2020). To elucidate the degradation patterns of sedimentary OC, organic geochemical biomarkers were utilized in this study. Our prior research revealed a clear decreasing trend in the abundance of nC_{14-35} alkanes and HMW *n*-alkanes in 2018 compared to 2006–2007, with reductions of 45.8% for nC_{14-35} alkanes and 49.1% for HMW *n*-alkanes (Wang et al., 2022a). The significant decrease in OC_{terr} content within surface sediments may create more adsorption sites for OC_{mar}, thereby augmenting the contribution of young OC_{mar}. Spatially, the distribution of CPI_{25-33} values (mean: 3.5 ± 1.3) exhibited higher values near the shore and lower values offshore (Fig. S4), indicating a greater maturity of sedimentary OC during lateral transport. Pearson correlation analysis revealed a strong relationship between $\Delta^{14}C$ values and CPI_{25-33} values (Fig. S5). In 2018, the spatial distribution of CPI_{25-33} values exhibited decreasing trends from the CRE region southward to the ZFCMB (Fig. S4), excluding the Yangtze Shoal. Furthermore, CPI_{25-33} values showed a strong positive correlation with the latitude of sampling sites in the mud deposits (Fig. S6), suggesting higher maturity of terrestrial sedimentary OC in the south compared to the north. Seabed erosion caused by hydrodynamics influences the maturity of terrestrial sedimentary OC due to both OC aging during lateral transport and the selective degradation of OC associated with sediment remobilization. The decreasing proportion of OC_{terr} and the superimposed degradation of OC_{terr} do not lead to the aging of sedimentary OC but may, in fact, result in a younger age by providing more adsorption sites for OC_{mar}. Additionally, debris from primary producers such as algae may also constitute an important component of OC_{mar}, which may not be easily preserved due to the lack of mineral protection.

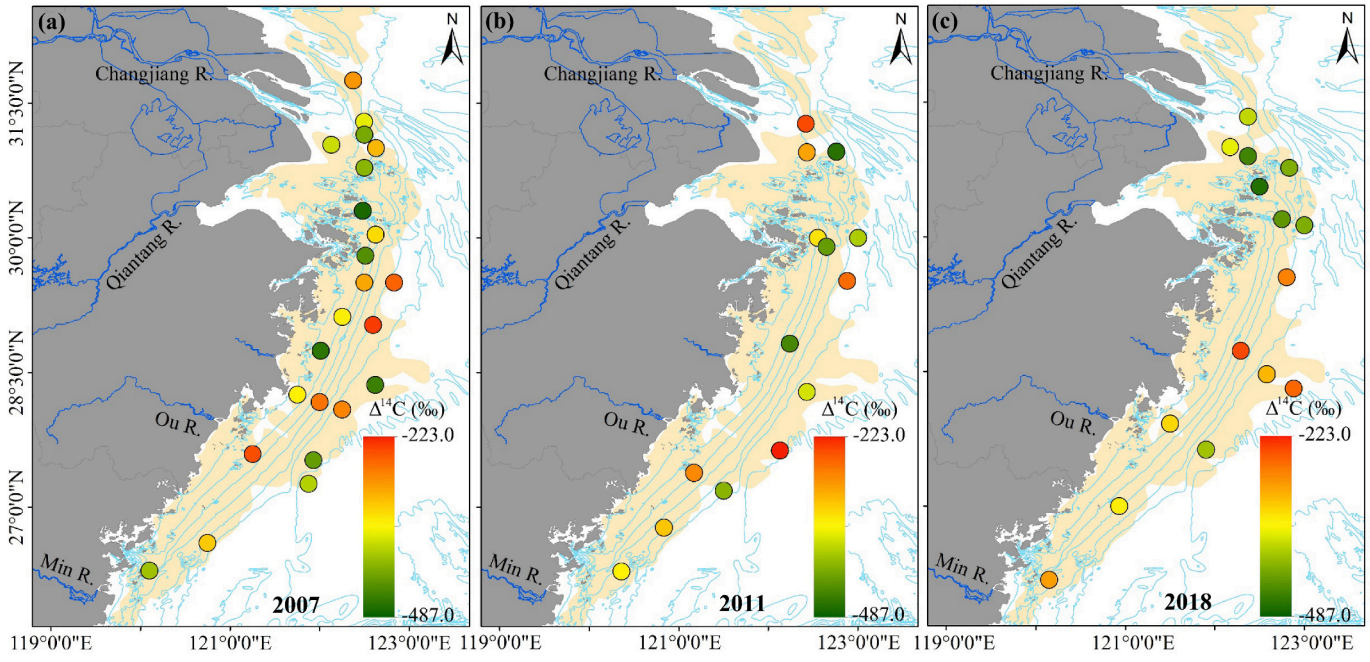
4.4. Is river damming responsible for younger sedimentary OC in the ECS?

Previous studies have indicated seabed erosion occurring in the estuarine-inner shelf areas of the ECS due to sediment reduction, resulting in significant sediment redistribution and coarsening (Yang et al., 2018; Gao et al., 2017, 2019). Moreover, these alterations notably impact the quantity and spatial distribution of sediment-associated organic matter, including organic pollutants and terrestrial biomarkers (Wang et al., 2020a, 2020b, 2020c, 2022a). Therefore, it is crucial to investigate whether variations in the sedimentary environment within the study area also influence $\Delta^{14}C$ values. The presence of strong correlations between $\Delta^{14}C$ values and mineral properties confirms that changes in the sedimentary environment can affect the spatial heterogeneity of $\Delta^{14}C$ values.

The mean $\Delta^{14}C$ values for surface sediments collected in 2007, 2011, and 2018 were − 376.3 ± 93.6‰, −327.6 ± 61.6‰, and − 348.6 ± 80.2‰, respectively. Results from the Shapiro-Wilk test indicate that all three sets of data do not conform to the normal distribution (all $p < 0.05$). The non-parametric Kruskal-Wallis test reveals no significant difference between the three groups of data (all $p > 0.05$). To further investigate the effects of river damming on the $\Delta^{14}C$ values, we narrowed the study area to the mud deposits affected by the Changjiang plume (Fig. 6). Shapiro-Wilk test results show that all three sets of data conform to the normal distribution (all $p > 0.05$). The $\Delta^{14}C$ values display an increasing trend across the three time periods (Fig. 6), with mean values of −354 ± 67‰, −321 ± 55‰, and − 306 ± 41‰, respectively ($F = 3.17$, $p = 0.05$). Spatially, the $\Delta^{14}C$ values for the three time periods were − 379 ± 60‰, −338 ± 63‰, and − 348 ± 29‰ in the CRE region (Fig. 6), which also conform to the normal distribution (Shapiro-Wilk test, all $p > 0.05$). However, the one-way ANOVA analysis shows no significant difference ($F = 0.97$, $p = 0.40$). The $\Delta^{14}C$ values in the ZFCMB for the three time periods were − 340 ± 66‰, −309 ± 44‰, and − 278 ± 18‰, respectively, displaying an increasing trend (Fig. 6, Shapiro-Wilk test, all $p > 0.05$; one-way ANOVA analysis: $F = 3.65$, $p = 0.04$).

The irregular variability of $\Delta^{14}C$ values in the inner CRE may be influenced by intensified vertical mixing processes resulting from a reduction in fluvial input (Fig. 7), consistent with the variation in excess ^{210}Pb activity reported by Gao et al. (2017). The increasing trend of $\Delta^{14}C$ values in the ZFCMB could be attributed to multiple factors. Firstly, the flux of riverine autochthonous OC has increased by 50% due to river damming, leading to the presence of younger OC_{terr} (Wang et al., 2022b). Additionally, sediment redistribution and coarsening inevitably induce the degradation of sedimentary OC_{terr}, potentially exposing more adsorption sites on particles. Consequently, with southward transport and the intense degradation of OC_{terr}, a greater amount of OC_{mar} becomes adsorbed onto the surface of particulates (Fig. 7b), contributing to the enrichment of $\Delta^{14}C$ values.

Although the mean $\Delta^{14}C$ values of the CRE region were higher than those of the ZFCMB in 2007 and 2011 (Fig. 6), the corresponding ANOVA results did not reach statistical significance (2007: $F = 1.18$, $p = 0.29$; 2011: $F = 0.48$, $p = 0.50$). However, in 2018, the mean $\Delta^{14}C$ values in the inner CRE were significantly lower than those in the ZFCMB ($F = 21.19$, $p < 0.05$). These variations may be attributed to the differential impacts of river damming on the fate of sedimentary OC during different periods. During the initial stages of damming, the sedimentary environment in the study area might not have undergone significant changes (Yang et al., 2018; Gao et al., 2019), thus the spatial variations of $\Delta^{14}C$ values within the study area might not have been significant either (Fig. 7a). However, as fluvial input continued to decrease over the long



(d)

	2007	2011	2018
Inner CRE	-379 ± 60‰	-338 ± 63‰	-348 ± 29‰
ZFCMB	-340 ± 66‰	-309 ±44‰	-278 ± 18‰

Fig. 6. Spatial distribution of $\Delta^{14}C$ values of sedimentary OC in the mud deposits, (a) 2007, (b) 2011, (c) 2018, (d) mean $\Delta^{14}C$ values of the ECS, north and south parts of mud deposits. The blue belt with gradient ramp showed the variation of $\Delta^{14}C$ values, with wide and light belt represent high value. (For interpretation of the references to colour in this figure legend, the reader is referred to the web version of this article.)

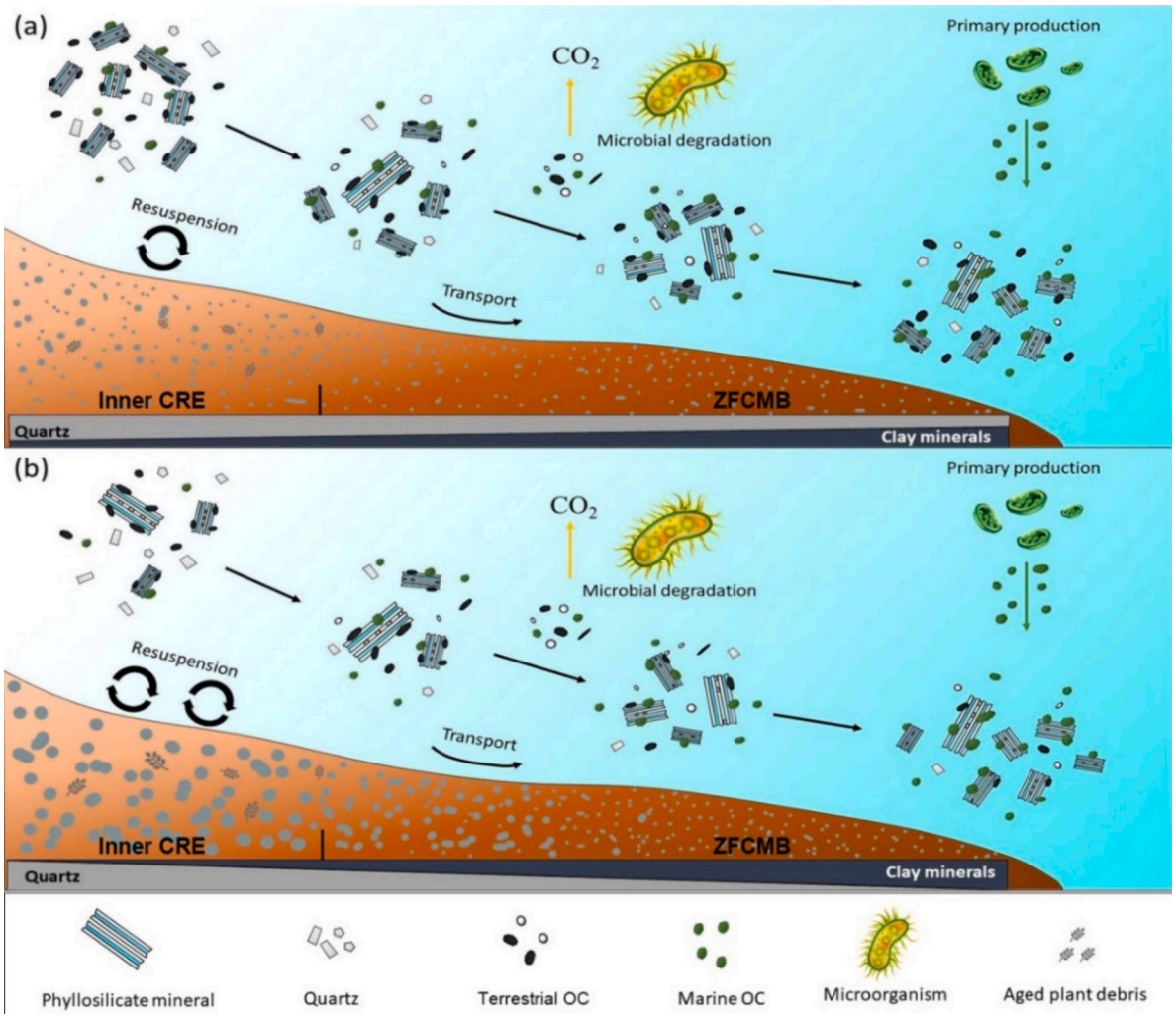


Fig. 7. Conceptual model showing the evolving OC-phyllosilicate associations across the fluvial-marine transition. Loss and replacement of aged OC_{terr} (black ellipses) with young OC_{mar} (green ellipses) during the southward transport from the inner CRE to the ZFCMB. (a) before river damming, (b) after river damming. (For interpretation of the references to colour in this figure legend, the reader is referred to the web version of this article.)

term, seabed erosion and sediment coarsening occurred (Fig. 7b), profoundly impacting the fate of sedimentary OC. The deposition flux of sedimentary OC in the study area decreased by nearly half due to the reduction of riverine input (Wang et al., 2020a). Presently, the deposition rate in the ECS has declined (Gao et al., 2019), leading to a longer oxygen exposure time for sediments, which may enhance the degradation of sedimentary OC, particularly Changjiang-derived terrestrial OC (OC_{terr}).

Similarly, deposition/resuspension loops resulting from seabed erosion also extend the oxygen exposure time for sedimentary OC. Furthermore, seabed erosion selectively removes significant amounts of fine-grained sediments while retaining coarse-grained sediments that offer less physical protection for OC. Consequently, as the southward transport distance increases, the degradation of OC_{terr} intensifies, resulting in the substitution of OC_{terr} with young OC_{mar} (Fig. 7b), thus influencing the spatial heterogeneity of $\Delta^{14}C$ values within the study area.

It is noteworthy that other RiOMars may also be facing similar threats. For instance, Syvitski et al. (2022) reported a 49% reduction in fluvial sediment reaching the oceans between 1950 and 2010 due to human activities, directly decreasing the flux of POC through riverine input. Additionally, the subaqueous deltas of major rivers such as the Mississippi and Yellow Rivers are experiencing retrogradation (Maloney et al., 2018; Liu et al., 2022), potentially altering the destiny of sedimentary OC in their adjacent coastal margins, akin to the ECS. Hence, further investigations are imperative to comprehend the ramifications of human disturbances on the fate of sedimentary OC in RiOMars.

5. Conclusions

Utilizing bulk OC properties, terrestrial biomarkers, and mineral properties, this study elucidates the origins and ages of sedimentary OC in the ECS and provides new insights into the factors influencing its fate. The $\Delta^{14}C$ values exhibit strong positive correlations with fine-grained sediments, SSA, and clay minerals (e.g., illite, chlorite, and kaolinite), indicating the significant role of mineral protection in regulating the fate of sedimentary OC. Our findings reveal a decrease in OC_{terr} content and an increase in OC_{mar} content during southward along-shelf transport, unveiling the variation pattern of OC sources during lateral transport in the ECS. We thus propose that the southward trend towards younger sedimentary OC may be attributed to the loss and replacement of OC_{terr} with OC_{mar} occurring during southward transport.

CRediT authorship contribution statement

Chenglong Wang: Writing – original draft, Methodology, Investigation, Funding acquisition, Conceptualization. **Chuchu Zhang:**

Visualization, Investigation, Formal analysis. **Zhuoyue Zhang:** Visualization, Software, Investigation. **Qihang Liao:** Visualization, Investigation, Formal analysis. **Yaping Wang:** Software, Methodology, Investigation, Formal analysis. **Xinqing Zou:** Writing – review & editing, Supervision, Project administration, Funding acquisition, Conceptualization.

Declaration of competing interest

The authors declare that they have no known competing financial interests or personal relationships that could have appeared to influence the work reported in this paper.

Data availability

The data used in our study was archived in an appropriate repository, which is available at https://zenodo.org/records/5761032.

Acknowledgements

The study was supported by the Natural Science Foundation of China (Grant Nos. 42106056) and the State Key Laboratory of Marine Geology, Tongji University (Grant Nos. MGK202410).

Appendix A. Supplementary data

Supplementary data to this article can be found online at https://doi.org/10.1016/j.margeo.2024.107322.

References

Ausín, B., Bruni, E., Haghipour, N., Welte, C., Eglinton, T., 2021. Controls on the abundance, provenance and age of organic carbon buried in continental margin sediments. Earth Planet. Sci. Lett. 558, 116759.
Bao, R., McIntyre, C., Zhao, M., Zhu, C., Kao, S.J., Eglinton, T., 2016. Widespread dispersal and aging of organic carbon in shallow marginal seas. Geology 44, 791–794.
Bao, R., McNichol, A., McIntyre, C., Xu, L., Eglinton, T., 2018a. Dimensions of radiocarbon variability within sedimentary organic matter. Radiocarbon 60 (3), 775–790.
Bao, R., van der Voort, T.S., Zhao, M., Guo, X., Montluçon, D.B., McIntyre, C., Eglinton, T., 2018b. Influence of hydrodynamic processes on the fate of sedimentary organic matter on continental margins. Glob. Biogeochem. Cycles 32, 1420–1432.
Bao, R., Blattmann, T.M., McIntyre, C., Zhao, M., Eglinton, T., 2019. Relationships between grain size and organic carbon ^{14}C heterogeneity in continental margin sediments. Earth Planet. Sci. Lett. 505, 76–85.
Bauer, J., Cai, W., Raymond, P., Bianchi, T., Hopkinson, C., Regnier, P., 2013. The changing carbon cycle of the coastal ocean. Nature 504, 61–70.
Bianchi, T., 2011. The role of terrestrially derived organic carbon in the coastal ocean: a changing paradigm and the priming effect. Proc. Natl. Acad. Sci. 108, 19473–19481.
Blair, N.E., Aller, R.C., 2012. The fate of terrestrial organic carbon in the marine environment. Annu. Rev. Mar. Sci. 4, 401–423.
Blattmann, T., Liu, Z., Zhang, Y., Zhao, Y., Haghipour, N., Montluçon, D.B., Plötze, M., Eglinton, T., 2019. Mineralogical control on the fate of continentally derived organic matter in the ocean. Science 366, 742–745.
Bouchez, J., Gaillardet, J., France-Lanord, C., Maurice, L., Dutra-Maia, P., 2011. Grain-size controls of river suspended sediment geochemistry: insights from Amazon River depth profiles. Geochem. Geophys. Geosyst. 2, GC00380.
Bröder, L., Tesi, T., Andersson, A., Semiletov, I., Gustafsson, Ö., 2018. Bounding cross-shelf transport time and degradation in Siberian-Arctic land-ocean carbon transfer. Nat. Commun. 9, 806.
Canuel, E.A., Hardison, A.K., 2016. Sources, ages, and alteration of organic matter in estuaries. Annu. Rev. Mar. Sci. 8, 409–434.
Carreira, R., Araújo, M., Costa, T., Spörl, G., Knoppers, B., 2011. Lipids in the sedimentary record as markers of the sources and deposition of organic matter in a tropical Brazilian estuarine-lagoon system. Mar. Chem. 127, 1–11.
Chen, Z., Zhou, C., Yang, W., Wu, Z., 1986. Subaqueous topography and sediments off modern Changjiang estuary. Donghai Mar. Sci. 4 (2), 28–37 (in Chinese).
Chen, Y., Chen, H., Gong, G., Lin, Y., Jan, S., Takahashi, M., 2004. Phytoplankton production during a summer coastal upwelling in the East China Sea. Cont. Shelf Res. 24, 1321–1338.
Chu, M., Zhao, M., Eglinton, T., Bao, R., 2022. Differentiating the causes of aged organic carbon in marine sediments. Geophys. Res. Lett. 49, e2021GL096912.
Drenzek, N., Montluçon, D., Yunker, M., Macdonald, R., Eglinton, T., 2007. Constraints on the origin of sedimentary organic carbon in the Beaufort Sea from coupled molecular 13C and 14C measurements. Mar. Chem. 103 (1–2), 146–162.
Eglinton, G., Hamilton, R.J., 1967. Leaf epicuticular waxes. Science 156, 1322–1335.
Fahl, K., Stein, R., 1997. Modern organic carbon deposition in the Laptev Sea and the adjacent continental slope: surface water productivity vs. terrigenous input. Org. Geochem. 26 (5–6), 379–390.
Fu, W., Xu, X., Druffel, E., Wang, X., Sun, S., et al., 2022. Carbon isotopic constraints on the degradation and sequestration of organic matter in river-influenced marginal sea sediments. Limnol. Oceanogr. 9999, 1–15.
Galy, V., Beyssac, O., France-Lanord, C., Eglinton, T., 2008. Recycling of graphite during Himalayan erosion: a geological stabilization of carbon in the crust. Science 322, 943–945.
Gao, J., Jia, J., Sheng, H., Yu, R., Li, G., Wang, Y., et al., 2017. Variations in the transport, distribution and budget of ^{210}Pb in sediment over the estuarine and inner shelf areas of the East China Sea due to Changjiang catchment changes. J. Geophy. Res. Earth 122, 235–247.
Gao, J., Jia, J., Kettner, A., Xing, F., Wang, Y., Li, J., et al., 2018. Reservoir-induced changes to fluvial fluxes and their downstream impacts on sedimentary processes: the Changjiang (Yangtze) River, China. Quat. Int. 493, 187–197.
Gao, J., Shi, Y., Sheng, H., Kettner, A.J., Yang, Y., Jia, J., Wang, Y., Li, J., Chen, Y., Zou, X., Gao, S., 2019. Rapid response of the Changjiang (Yangtze) River and East China Sea source-to-sink conveying system to human induced catchment perturbations. Mar. Geol. 414, 1–17.
Guo, L., Su, N., Ian, T., Wang, Z., Zhu, C., Zhang, Y., Wang, X., He, Q., 2019. From the headwater to the delta: a synthesis of the basin-scale sediment load regime in the Changjiang River. Earth-Sci. Revi. 197, 102900.
Hemingway, J., Rothman, D., Grant, K.E., Rosengard, S., Eglinton, T., Derry, L., Galy, V., 2019. Mineral protection regulates long-term global preservation of natural organic carbon. Nature 570, 228–231.
Hu, J., Wang, X., 2016. Progress on upwelling studies in the China seas. Rev. Geophys. 54, 653–673.
Hu, L., Shi, X., Yu, Z., Lin, T., Wang, H., Ma, D., Guo, Z., Yang, Z., 2012. Distribution of sedimentary organic matter in estuarine-inner shelf regions of the East China Sea: Implications for hydrodynamic forces and anthropogenic impact. Mar. Chem. 142, 29–40.
Huguet, C., de Lange, G., Gustafsson, Ö., Middelburg, J., Sinninghe Damsté, J., Schouten, S., 2008. Selective preservation of soil organic matter in oxidized marine sediments (Madeira Abyssal Plain). Geochim. Cosmochim. Acta 72, 6061–6068.
Kao, S., Hilton, R., Selvaraj, K., Dai, M., Zehetner, F., Huang, J., Hsu, S., Sparkes, R., Liu, J., Lee, T., Yang, J., Galy, A., Xu, X., Hovius, N., 2014. Preservation of terrestrial organic carbon in marine sediments offshore Taiwan: mountain building and atmospheric carbon dioxide sequestration. Earth. Surf. Dyn. 2, 127–139.
Karlsson, E., Brüchert, V., Tesi, T., Charkin, A., Dudarev, O., Semiletov, I., Gustafsson, Ö., 2015. Contrasting regimes for organic matter degradation in the East Siberian Sea and the Laptev Sea assessed through microbial incubations and molecular markers. Mar. Chem. 170, 11–22.
Li, G., Li, P., Liu, Y., Qiao, L., Ma, Y., Xu, J., Yang, Z., 2014a. Sedimentary system response to the global sea level change in the East China Seas since the last glacial maximum. Earth-Sci. Revi. 139, 390–405.
Li, D., Yao, P., Bianchi, T., Zhang, T., Zhao, B., Pan, H., Wang, J., Yu, Z., 2014b. Organic carbon cycling in sediments of the Changjiang Estuary and adjacent shelf: Implication for the influence of Three Gorges Dam. J. Mar. Syst. 2014 (139), 409–419.
Lin, T., Hu, L., Guo, Z., Zhang, G., Yang, Z., 2013. Deposition fluxes and fate of polycyclic aromatic hydrocarbons in the Yangtze River estuarine-inner shelf in the East China Sea. Glob. Biogeochem. Cycles 27 (1), 77–87.
Liu, J., Xu, K., Li, A., Milliman, J., Velozzi, D., Xiao, S., Yang, Z., 2007. Flux and fate of Yangtze River sediment delivered to the East China Sea. Geomorphology 85, 208–224.
Liu, J., Qiu, J., Saito, Y., Zhang, X., Nian, X., Wang, F., Xu, G., Xu, T., Li, M., 2020. Formation of the Yangtze Shoal in response to the post-glacial transgression of the paleo-Yangtze (Changjiang) estuary, China. Mar. Geol. 423, 106080.
Liu, L., Wang, H., Yang, Z., Fan, Y., Wu, X., Hu, L., Bi, N., 2022. Coarsening of sediments from the Huanghe (Yellow River) delta-coast and its environmental implications. Geomorphology 401, 108105.
Ludwig, W., Probst, J., Kempe, S., 1996. Predicting the oceanic input of organic carbon by continental erosion. Glob. Biogeochem. Cycles 10 (1), 23–41.
Maavara, T., Lauerwald, R., Regnier, P., Cappellen, P., 2017. Global perturbation of organic carbon cycling by river damming. Nat. Commun. 8, 15347.
Maloney, J., Bentley, S., Xu, K., Obelcz, J., Georgiou, I., Miner, M., 2018. Mississippi river subaqueous delta is entering a stage of retrogradation. Mar. Geol. 400, 12–23.
Regnier, P., Friedlingstein, P., Ciais, P., Mackenzie, F.T., Gruber, N., Janssens, I.A., Laruelle, G.G., Lauerwald, R., Luyssaert, S., Andersson, A.J., Arndt, S., Arnosti, C., Borges, A.V., Dale, A.W., Gallego-Sala, A., Goddéris, Y., Goossens, N., Hartmann, J., Heinze, C., Ilyina, T., Joos, F., LaRowe, D.E., Leifeld, J., Meysman, F.J.R., Munhoven, G., Raymond, P.A., Spahni, R., Suntharalingam, P., Thullner, M., 2013. Anthropogenic perturbation of the carbon fluxes from land to ocean. Nat. Geosci. 6, 597–607.
Stuiver, M., Polach, H., 1977. Discussion: reporting of C-14 data. Radiocaron 19 (3), 355–363.
Sun, X., Fan, D., Cheng, P., Hu, L., Sun, X., Guo, Z., Yang, Z., 2021. Source, transport and fate of terrestrial organic carbon from Yangtze River during a large flood event: insights from multiple-isotopes (δ^{13}C, δ^{15}N, Δ^{14}C) and geochemical tracers. Geochim. Cosmochim. Acta 308, 217–236.
Sun, X., Fan, D., Hu, L., Yang, Z., Guo, Z., 2022. Oxidation of petrogenic organic carbon in a large river-dominated estuary. Geochim. Cosmochim. Acta 338, 136–153.
Syvitski, J., Ángel, J., Saito, Y., Overeem, I., Vörösmarty, C., Wang, H., Olago, D., 2022. Earth's sediment cycle during the Anthropocene. Nat. Rev. Earth. Env. 3, 179–196.

van der Voort, T., Mannu, U., Blattmann, T., Bao, R., Zhao, M., Eglinton, T., 2018. Deconvolving the fate of carbon in coastal sediments. Geophys. Res. Lett. 45 (9), 4134–4142.
Vonk, J., Sanchez-Garcia, L., van Dongen, B., Alling, V., Kosmach, D., Charkin, A., Semiletov, I., Dudarev, O., Shakhova, N., Roos, P., Eglinton, T., Andersson, A., Gustafsson, O., 2012. Activation of old carbon by erosion of coastal and subsea permafrost in Arctic Siberia. Nature 489 (7414), 137–140.
Wang, X., Ma, H., Li, R., Song, Z., Wu, J., 2012. Seasonal fluxes and source variation of organic carbon transported by two major Chinese Rivers: the Yellow River and Changjiang (Yangtze) River. Glob. Biogeochem. Cycles 26, GB2025.
Wang, H., Dai, M., Liu, J., Kao, S., Zhang, C., Cai, W., Wang, G., Qian, W., Zhao, M., Sun, Z., 2016. Eutrophication-Driven Hypoxia in the East China Sea off the Changjiang Estuary. Environ. Sci. Technol. 50, 2255–2263.
Wang, C., Hao, Z., Gao, J., Feng, Z., Ding, Y., Zhang, C., Zou, X., 2020a. Reservoir construction has reduced organic carbon deposition in the East China Sea by half since 2006. Geophys. Res. Lett. 47, e2020GL087357.
Wang, C., Hao, Z., Feng, Z., Zhang, C., Li, Y., Yu, W., Zou, X., 2020b. Shifts in the distribution and fate of sedimentary polycyclic aromatic hydrocarbons within the estuarine-inner shelf areas of the East China Sea: response to human-induced catchment change. J. Geophys. Res. Oceans 125, e2019JC015773.
Wang, C., Hao, Z., Feng, Z., Zhang, C., Zou, X., 2020c. Rapid changes in organochlorine pesticides in sediments from the East China Sea and their response to human-induced catchment changes. Water Res. 169, 115225.
Wang, C., Zhang, C., Wang, Y., Jia, G., Wang, Y., Zhu, C., Yu, Q., Zou, X., 2022a. Anthropogenic perturbations to the fate of terrestrial organic matter in a river-dominated marginal sea. Geochim. Cosmochim. Acta 333, 242–262.
Wang, H., Ran, X., Bouwman, A., Wang, J., Xu, B., Song, Z., Sun, S., Yao, Q., Yu, Z., 2022b. Damming alters the particulate organic carbon sources, burial, export and estuarine biogeochemistry of rivers. J. Hydrol. 607, 127525.
Wei, B., Mollenhauer, G., Hefter, J., Grotheer, H., Jia, G., 2020. Dispersal and aging of terrigenous organic matter in the Pearl River Estuary and the northern South China Sea Shelf. Geochim. Cosmochim. Acta 282, 324–339.
Wu, Y., Eglinton, T., Yang, L., Deng, B., Montluçon, D., Zhang, J., 2013. Spatial variability in the abundance, composition, and age of organic matter in surficial sediments of the East China Sea. Eur. J. Vasc. Endovasc. Surg. 118, 1495–1507.
Xu, X., Trumbore, S., Zheng, S., Southon, J., et al., 2007. Modifying a sealed tube zinc reduction method for preparation of AMS graphite targets: reducing background and attaining high precision. Nucl. Instrum. Meth. B 259 (1), 320–329.
Yang, S., Milliman, J., Li, P., Xu, K., 2011. 50,000 dams later: erosion of the Yangtze River and its delta. Glob. Planet. Chang. 75 (1–2), 1–20.
Yang, H., Yang, S., Meng, Y., Xu, K., Luo, X., Wu, C., et al., 2018. Recent coarsening of sediments on the southern Yangtze subaqueous delta front: a response to river damming. Cont. Shelf Res. 155, 45–51.
Yao, P., Yu, Z., Bianchi, T., Guo, Z., Zhao, M., Knappy, C., Keely, B., Zhao, B., Zhang, T., Pan, H., Wang, J., Li, D., 2015. A multiproxy analysis of sedimentary organic carbon in the Changjiang Estuary and adjacent shelf. Eur. J. Vasc. Endovasc. Surg. 120, 1407–1429.
Yuan, D., Hsueh, Y., 2010. Dynamics of the cross-shelf circulation in the Yellow and East China Seas in winter. Deep. Sea. Res. PT II 57 (19–20), 1745–1761.
Zhao, B., Yao, P., Bianchi, T., Wang, X., Shields, M., Schröder, C., Yu, Z., 2023. Preferential preservation of pre-aged terrestrial organic carbon by reactive iron in estuarine particles and coastal sediments of a large river-dominated estuary. Geochim. Cosmochim. Acta 345, 34–49.
Zhu, Z., Zhang, J., Wu, Y., Zhang, Y., Lin, J., Liu, S., 2011. Hypoxia off the Changjiang (Yangtze river) estuary: oxygen depletion and organic matter decomposition. Mar. Chem. 125, 108–116.
Zhu, S., Ding, P., Wang, N., Shen, C., Jia, G., Zhang, G., 2015. The compact AMS facility at Guangzhou Institute of Geochemistry, Chinese Academy of Sciences. Nucl. Instrum. Meth. B 361, 72–75.